NASA Technical Memorandum 82990

Improved Ion Containment Using a Ring-Cusp Ion Thruster

J. S. Sovey
Lewis Research Center
Cleveland, Ohio

Prepared for the
Sixteenth International Electric Propulsion Conference
cosponsored by the American Institute of Aeronautics and Astronautics,
the Japan Society for Aeronautical and Space Sciences,
and Deutsche Gesselschaft fur Luft- und Raumfahrt
New Orleans, Louisiana, November 17-19, 1982

NASA

E-1422

IMPROVED ION CONTAINMENT USING A RING-CUSP ION THRUSTER

J. S. Sovey

National Aeronautics and Space Administration
Lewis Research Center
Cleveland, Ohio 44135

ABSTRACT

A 30-centimeter diameter ring-cusp ion thruster is described which operates at inert gas ion beam currents up to about 7 amperes, with significant improvements in discharge chamber performance over conventional divergent-field thrusters. The thruster has strong boundary ring-cusp magnetic fields, a diverging field in the cathode region, and a nearly field-free volume upstream of the ion extraction system. Minimum ion beam production costs of 90 to 100 watts per beam ampere were obtained for argon, krypton and xenon. Propellant efficiencies in excess of 0.90 were achieved at 100 to 120 watts per beam ampere for the three inert gases. The ion beam charge-state was documented with a collimating mass spectrometer probe to allow evaluation of overall thruster efficiencies.

SYMBOLS

A	accelerator grid open area, cm^2
d	ion extraction diameter, cm
e	electronic change, 1.6×10^{-19} C
F_T	thrust reduction factor due to beam divergence
g	gravity acceleration, 9.8 m/s^2
I_{sp}	specific impulse, s
I^{+}_{++}	mass spectrometer singly-charged ion current, A
I^{++}	mass spectrometer doubly-charged ion current, A
I^{+++}	mass spectrometer triply-charged ion current, A
J_B	ion beam current, A
J_C	cathode current, A
J_D	discharge (anode) current, A
J_G	grid ion current, A (ref. Tables II,III)
l	effective discharge chamber length, cm
M	propellant molecular weight, kg
$\dot{M}_O$	total mass flow rate, kg/s
M_W	propellant molecular weight, amu
$\dot{m}_B$	ionized mass flow rate, A
$\dot{m}_C$	cathode flow rate, A
$\dot{m}_I$	ingested gas flow rate, A
$\dot{m}_M$	main feed ring flow rate, A
$\dot{m}_N$	neutralizer flow rate, A
$\dot{m}_O$	total mass flow rate, A

*AIAA Paper No. 82-1928.

P	thruster input power, w
P_F	fixed power loss due to accelerator grid power supply, neutralizer, and heaters, w
p	vacuum facility pressure corrected for type of gas, Pa
R	ratio of doubly to singly-charged ion currents
T_A	actual thrust, N
T_I	ideal thrust, N
V_B	ion beam voltage, $V_B \approx V_S + V_D - V_N$, V
V_D	discharge (anode) voltage (relative to cathode potential), V
V_N	neutralizer floating voltage (relative to ground), V
V_S	screen power supply voltage (relative to neutralizer potential), V
α	thrust-correction factor due to multiply-charged ions
β	ionized mass flow rate correction factor
γ	overall thrust correction factor
ϵ	ion beam production cost, watts per beam ampere (W/A)
η_T	overall thruster efficiency
η_u	propellant efficiency corrected for multiply-charged ions, $\beta J_B/\dot{m}_0$
η'_u	propellant efficiency uncorrected for multiply-charged ions
η_{uD}	discharge chamber propellant efficiency corrected for multiply-charged ions, $\beta J_B/(\dot{m}_0-\dot{m}_N)$
η'_{uD}	discharge chamber propellant efficiency uncorrected for multiply-charged ions

INTRODUCTION

Ion-thruster systems are candidates for on-orbit propulsion functions and orbit transfer of large space systems. Analyses have shown that thruster characteristics, such as type of propellant, thrust density, and overall thruster efficiency, are crucial to key system parameters such as thrust to power ratio, system mass, and power requirements. These parameters, in turn, strongly impact major mission characteristics such as thrusting time, system cost, and payload capability. Previously, the major obstacle to improved inert gas thruster performance was the relatively high ion beam production cost which degraded performance in the specific impulse range of 2000 to 5000 sec. Reduced ion production costs would improve thruster performance and benefit the thruster thermal design and component lifetime because of lower discharge power demands.

Recent investigations have pursued performance documentation and optimization of inert gas ion thrusters, (refs. 1, 2, and 3). Such thrusters employed divergent magnetic fields, as well as line and ring-cusp configurations. These devices have exhibited ion beam production costs in excess of 150 watts per beam ampere (W/A) and, in some cases, could not obtain argon propellant efficiencies in excess of 0.80.

This paper describes efforts to reduce the ion-beam production costs of multicusp ion thrusters, while simultaneously enabling propellant efficiencies in excess of 0.90. The ring-cusp thrusters described herein used a number of the discharge-chamber features contained in the magneto-electrostatic containment ion thruster, reported by Moore in 1969 (ref. 4). Initial experiments were conducted with line-cusp devices followed by tests of ring-cusp thrusters with a shell anode configuration. Efforts were undertaken to optimize the diverging magnetic field in the cathode region and the strong ring-cusp boundary fields to produce low ion wall losses in

the chamber and enhance the forward ion flux. Finally, mass spectrometer data were obtained to determine the charge state of the argon, xenon, and krypton ion beams to allow correction of the metered performance values.

APPARATUS AND PROCEDURE

A schematic of a typical ring-cusp thruster is shown in figure 1. The figure displays a sketch of an iron filing map showing a diverging field at the cathode produced by an Alnico cylindrical magnet. Also shown is the strong coupling of the cathode magnet field to the magnet ring near the middle of the chamber. Strong boundary fields were produced by samarium-cobalt magnets whose dimensions were 1.3 by 1.9 by 0.5 cm. The magnets, when placed on the iron anode, produced about 0.24 T at their surface. In order to maintain test flexibility, no attempt was made to cover the magnets. For laboratory expedience, the anode shell was water-cooled to prevent irreversible losses of magnet properties at temperatures exceeding 300° C at high discharge powers.

Figure 2 shows the magnetic-field contours of a typical ring-cusp device. The axial magnetic field varies from about 20 mT at the cathode tip to less than 0.5 mT at the ion-extraction plane. Also shown is a rather large volume where the resultant magnetic field is less than 2 mT. A downstream pole piece, at anode potential, was used to terminate the magnetic field lines upstream of the ion optics.

The line-cusp thrusters contained an iron-cylindrical shell and a flat backplate which were at anode potential. Either 12, 16, or 24 equally-spaced rows of magnets were placed on the iron-cylindrical shell. The magnet rows were terminated on the backplate using the method shown in note (b) of table I. The cathode assembly was identical to the one used on the ring-cusp device and the cathode magnet was moved axially to give the desired magnetic field at the cathode tip.

Table I shows the detailed design information for several versions of line-cusp and ring-cusp discharge chambers. These devices were usually operated with the cylindrical shell, backplate, and downstream pole piece at anode potential. Some early tests used the line-cusp configuration, but most of the effort was devoted to the ring-cusp-type chambers. The ring-cusp devices combine three functions used in various types of ion sources to reduce ion wall losses and promote a forward ion flux by adjustment of the magnetic field at the cathode and shell boundary. The three basic magnetic circuit features include a multicusp boundary field with an anode shell (refs. 2 and 5), a hollow cathode/magnet assembly (refs. 3, 4), and the downstream anode pole piece.

Thrusters LCI and RCI had ion-extraction diameters that were only 26 cm, thus full advantage was not taken of the ion optics' 28.3 cm ion-extraction diameter. Subsequent thrusters were constructed using a 34 cm-diameter shell. Most of the optimization efforts used thrusters of type RC2.

Gas was admitted into the chamber through the hollow cathode and through a perforated main gas-feed ring. Typical cathode flow rates for argon, krypton, and xenon were 0.7, 0.4, and 0.2 equivalent amperes, respectively. These cathode flow rates generally maintained discharge voltages of argon,

krypton, and xenon to less than 50, 45, and 40 V, respectively. The 6.4-mm-diameter hollow cathode had a 1-mm-diameter chambered orifice with a 0.5-mm-long throat (ref. 2). The discharge was initiated by applying a high-voltage pulse between the starting electrode and the cathode. Ions were extracted using a dished ion-optical system with screen and accelerator grid open area fractions of 0.75 and 0.29, respectively (refs. 2 and 6). Grid-to-grid spacing was approximately 0.7-mm. Typical screen and accelerator grid voltages were, respectively, +1400 and -500 V.

A 6.4-mm-diameter hollow cathode neutralizer was used with an enclosed keeper electrode spaced 1.2 cm from the cathode. The neutralizer was located 10 cm axially and 10 cm radially from the last row of grid holes (ref. 2).

Thruster performance evaluation with ion extraction was conducted in a 4.6- by 19.2-m-long vacuum facility. Operating vacuum-facility pressures were generally less than 2×10^{-3} Pa (1.5×10^{-5} torr). Gas flow rates were measured with mass flow rate transducers which were calibrated with argon using volume-displacement methods. Flow rate calibrations for xenon and krypton were obtained using gas-conversion factors supplied by the transducer vendor. All data presented were corrected for gas ingested from the vacuum facility. The equation used to calculate ingestion, for an inert gas thruster was

$$\dot{m}_I = 2.0 \frac{pA}{\sqrt{M_W}} \tag{1}$$

All symbols are defined in the symbol list. This calculation assumes molecular flow through the downstream grid orifices into a discharge chamber with zero pressure. There are relatively few heavy particle collisions since the argon molecular mean free path is >6 cm at discharge chamber pressures <0.1 Pa. Typical ingested flow rates were 0.08, 0.05 and 0.06 A for argon, krypton, and xenon respectively, for tests with ion extraction.

The indicated ion beam current was corrected for multiply charged ions, using an ExB mass spectrometer probe, fabricated by Xerox Electro-Optical Systems. The probe was similar to the device described in reference 7. The probe had a double-collimating orifice system, producing very high angular resolution at a position 15 cm downstream of the ion optics. The ion current collected was from a single grid aperature and possibly its nearest neighbors. Worst-case corrections to the ion beam current were made by assuming the ratio of doubly (or triply) ionized species to singly ionized species, equal to the maximum values observed at the centerline of the thruster.

Many of the early thruster-optimization efforts were done without ion extraction in a smaller vacuum facility to expedite testing. In this facility, typical argon flow rates through the cathode, the main feed ring, and facility gas injestion were approximately 1.3, 6, and 6 A, respectively. The downstream end of the discharge chamber was terminated with a single, stainless steel grid with an exhaust diameter of 28.3 cm and an open area fraction of 0.23. The grid was operated at cathode potential. To monitor radial variations in the ion current density, three planar probes were

mounted from the grid on the centerline and at radial locations of 6.2 and 12.4 cm. Azimuthal symmetry at the grid plane was assumed. Planar probes were also mounted on magnets and discharge chamber walls to monitor ion and electron currents to these surfaces. All of the probes were typically 1.3 cm diameter and were biased at -35 V with respect to the cathode, for ion collection and at anode potential for electron collection. Variations in discharge-chamber magnetic configurations and geometries were evaluated by comparing values of integrated ion current at the ion extration plane and by metering ion currents to the chamber surfaces. It was the intention of the optimization effort to increase the ion flux directed toward the extraction plane, and decrease the ion currents to the discharge chamber walls to reduce the ion-beam production costs and increase propellant efficiency.

RESULTS AND DISCUSSION

The results of this experimental program to improve the ionization and propellant efficiency of multicusp ion thrusters are presented. Most of the efforts dealing with variations in magnetic configuration and chamber geometry were done without high voltage ion-extraction because a smaller vacuum facility was more accessible, and experiment modification could be made rapidly. Thruster-performance evaluation with ion extraction generally requires background pressures of about 2×10^{-3} Pa (1.5×10^{-5} torr) or lower, so that thruster gas-ingestion and accelerator grid charge exchange are not major effects. The basis for performance comparison in tests without ion extraction was the integrated ion current at the grid plane. The most promising configurations were evaluated with ion extraction for performance and ion-beam change-state documentation.

Thruster Performance without Ion Extraction

A variety of experiments were undertaken to compare performance of thruster configurations based on the ion current passing to the grid plane. An integrated value of ion current was obtained for each configuration based on the data from the three biased-grid probes. All thruster operation described in this section was performed with argon gas.

The discharge parameters can vary significantly in situations with and without ion extraction. For example, the discharge impedance, at propellant efficiencies in excess of 0.90, can be 10 to 40 percent higher with ion extraction. Even though the plasma characteristics differ, depending whether or not ions are extracted at high voltage, it is assumed that performance trends are similar, independent of the use of two-grid ion extraction or a single-grid operation. Some evidence to support this premise will be shown in a subsequent section.

Early experiments were conducted to compare line-cusp thruster performance. The integrated ion current to the grid place for LC2 and LC3, which had 24 and 16 magnet rows, respectively, was about the same (table II), indicating there was probably no significant reduction in cusp-loss currents by reducing the number of magnet rows. Thruster LC2 had a more uniform ion-current profile at the grid plane since the larger number of magnet rows produced boundary fields that did not penetrate radially as much as configuration LC3. These line-cusp devices produced grid-plane ion currents that

were about 20 percent lower than the basic ring-cusp thruster, RC2. By going to the ring-cusp design, the ion currents to the anode cylindrical shell and backplate were reduced by at least a factor of two. This result prompted further exploration of other ring-cusp configurations.

Nearly all of the ring-cusp devices had two rings of magnets on the iron backplate. Reduction of the number of rings in the cylindrical shell of thruster RC2 from six to two resulted in nearly the same grid-place ion flux, as long as the downstream ring of magnets was bout 4 cm from the end of the shell. A 10-percent reduction in grid-plane ion current and a more peaked radial profile resulted if the downstream ring of magnets was moved 8 cm from the end of the shell. The configuration RC2 was preferred because thrusters with four or six rings of magnets in the iron cylinder produced discharge voltage in excess of 50 V at discharge currents of 10 A or less.

The cathode-magnet assembly of thruster RC2 was moved upstream 2.5 cm without any change in the grid-plane ion current. Other variations in this parameter were not made because of hardware limitations.

There were insignificant changes in the grid plane ion current of RC2 when operated with or without the downstream pole piece. The downstream pole piece did produce a 7 percent increase in forward ion current using RC1 and also increased peripheral ion current density. The pole piece apparently provided needed coupling of field lines from the downstream magnet ring, which was 6.2 cm from the end of the shell of thruster RC1 compared with only 3.8 cm for thruster RC2.

Attempts were made to increase the ion current to the thruster grid plane by increasing the magnetic field strength at selected ring cusps and by adding a ring of magnets to the downstream pole piece. By simply adding another layer of magnets to a ring, the average field at the magnet face increased from 0.24 to 0.32 T. Increasing the field at the cusp on the two downstream rings of RC2 resulted in an extremely peaked grid-plane current profile and very little gain in total ion current.

Table II shows quantitative results of some of the basic thruster modifications that resulted in increased grid-plane ion current and more uniform ion-density profiles. The measure of the ion-density uniformity has been called the flatness parameter and is defined to be the ratio of average to centerline ion-current density. All comparisons were made at a discharge voltage of 40 V and a total argon flow rate estimated to be about 13 A. The sum of the cathode and grid currents was held at 42A.

First, the field strength of the four upstream magnet rings was increased to 0.32 T, (RC2, Mod. 1), which resulted in an 11 percent increase in total ion current. By increasing the magnetic field strength in the rear of the chamber, the flatness of the ion-density profile was also improved. The next iteration simply involved adding a ring of magnets to the downstream pole piece of RC2; this configuration is referred to as RC3. There was no gain in total ion current, but the ratio of average to centerline ion-current density increased from 0.61 to 0.76.

The RC3 configuration was modified to increase the grid-plane ion current. The field strength of the four upstream magnet rings was increased

to 0.32 T for Mod 1. The grid-plane ion current increased by 16 percent over that of the RC2 thruster, but the flatness parameter decreased from 0.76 to 0.67. The final configuration, RC3, Mod. 2, had 0.32 T at the face of magnets on the three upstream rings, and 0.24 T for the two downstream rings as well as the ring of magnets on the downstream pole piece. The ion current to the grid plane in this case was 16.9 A, compared with 14.6 A for thruster RC_2, a 16 percent increase. The gain in grid plane ion current was accomplished at a cathode current about 2A lower than used in the thruster RC_2. In addition, the RC3, Mod. 2 discharge chamber had the highest flatness parameter, 0.80.

In summarizing the results of table II, the gains in grid-plane ion current were accomplished by increasing the field strength of the upstream magnet rings. The increased magnet ring-field strength on the backplate also increased the axial magnetic field strength at the cathode by about 50 percent (table I). Improvements in ion-current profile flatness parameter were achieved by adding a ring of magnets to the downstream pole piece or by increasing the magnet-ring field strength in the rear of the chamber. The magnet ring on the downstream pole piece must be properly located because small reductions in the ring diameter significantly reduced the flatness parameter.

Table III shows the typical ion and electron current distribution in the chamber and at the grid of RC3, Mod. 2 The current densities in the cusp regions were probably very high because ion etch marks on the magnets indicate cusp widths from 0.5 to 2 mm. Most of the probe measurements were taken at 1.8 cm above the chamber surface. Comparing the data of probes 5 and 7, the measurements taken 1.2 cm above the magnet surface were not indicative of wall currents and were high by a factor of two to three. Table III shows that the ion current to the anode wall between cusps is less than 7 percent of ion current directed toward the center of the grid. The value of ion current to the backplate is less than 2 percent of the forward ion current. Estimated ion current densities, at a cathode current of about 25A, are about 30 mA/cm^2 at the center of the grid plane, 20 to 80 mA/cm^2 at the narrow magnetic cusps of the two downstream rings, and less than 1 mA/cm^2 to the walls. The planar probe data indicate the desirable features of the high forward ion current and the low wall losses and also point out that attention should be paid to examination of ion erosion sites at the screen grid and magnet cusp areas. Based on the integrated probe data of the thruster described in table III, an ion beam production cost was estimated to be about 85 W/A, assuming an 80 percent ion optics effective transparency. This may not be an effective method of estimating ion beam production costs since ions are not as efficiently swept out of the chamber, as is the case with high voltage ion extraction. The thruster could certainly be further improved by reducing the 1.6 A ion current to the downstream pole piece. This current is nearly 10 percent of the grid plane ion current.

Nearly all of the electron currents were collected by the two downstream magnet rings and the downstream pole piece. The net electron-current density to the narrow cusps of the two downstream rings of RC3, Mod. 2, is estimated to be between 1 and 5 A/cm^2 at a cathode current of 25A. The downstream pole piece received about 10 A net electron current. This pole piece serves as additional anode area and when a ring of magnets was mounted

to it, a higher grid-plane ion-current flatness parameter resulted. Small variations in this magnet ring diameter affected the flatness parameter markedly. Operating the downstream pole piece at cathode potential produced an undesirable increase in discharge voltage from 30 to about 52 V, at a 25A cathode current.

Ion-Beam Charge State Documentation

Ion-beam charge state data are needed to correct the metered performance parameters for multiply charged ion species and also to determine values of discharge voltage and current that are consistent with long component lifetime. Data were obtained using an ExB spectrometer probe located approximately 15 cm downstream of thruster RC3. In nearly all cases data were taken only on the thruster centerline.

Figure 3 shows the variation of the ratio of doubly to singly charged ions over a range of discharge voltage from 27 to 62 V. Argon discharge voltages less than 36 V produced a ratio of doubly to singly charged ions that was less than 1 percent. At the same discharge voltage, krypton and xenon propellants exhibited ratios of 9 and 17 percent, respectively.

There was no evidence of triply charged argon ions at discharge voltages up to 62 V and discharge powers up to 1100 W. However, triply charged xenon and krypton ions, which were one to 2 percent of the single ionized species, were observed at 42 and 46 V, respectively. Figure 4 shows the dependence of the centerline value of the ion mass flow rate correction factor for multiply charged ions, β, versus measured propellant efficiency. The measured propellant efficiency, η'_{UD}, is the metered ion-beam current divided by the gas flow rate (in amperes), into the discharge chamber. The ionized mass flow rate expressed in equivalent amperes is

$$\dot{m}_B = \beta J_B \tag{2}$$

$$\beta = \frac{I^{+} + \left(\frac{1}{2}\right) I^{++} + \left(\frac{1}{3}\right) I^{++}}{I^{+} + I^{++} + I^{+++}} \tag{3}$$

where I^{+}, I^{++}, and I^{+++} are the spectrometer currents associated with singly, doubly, and triply charged beam ions. Because extensive radial probe data were not taken, the propellant efficiency values, η_{UD}, of all data presented were corrected assuming the average β is equal to the centerline value. This procedure results in a worst-case correction. The data of figure 4 indicate a good correlation between β and measured propellant efficiency, η'_{UD}, for the gases argon, krypton, and xenon, with a given thruster configuration. Estimates of ion-mass flow rate correction factors might simply be obtained by using the relationship between β and measured propellant efficiency, rather than performing extensive spectrometer probe measurements. Similar charge-state parameter correlations were performed with mercury ion thrusters (ref. 8).

Table IV shows the radial variation of I^{++}/I^{+} for selected operating values of argon and xenon thrusters. Also shown are the I^{++}/I^{+} values which were simply obtained by averaging over the ion optics area.

The measured beam currents for both propellants were 4.9 A. The discharge voltage for xenon was rather high (41.5 V) and the average ratio of I^{++}/I^{+} was 0.22, which was a factor of 1.6 lower than the centerline value. The argon thruster had an average of I^{++}/I^{+} which was a factor of 1.3 lower than the centerline value. Divergent-field mercury thrusters have centerline values of I^{++}/I^{+} that were factors of two to three higher than the average values at propellant efficiencies comparable to the inert gas ring-cusp thruster (ref. 8). Given comparable discharge parameters, the inert gas ring-cusp thruster should exhibit less ion-optics grid erosion than the divergent field thruster because of a relatively lower concentration of double charged ions on centerline. Potential erosion problems may, however, exist with argon propellant, due to the relatively high sputter yield, when compared with heavier ions like mercury or xenon (ref. 1).

The sensitivity of applying the centerline versus average value of β to the calculation of m_β, and n_{0D} can be assessed by first assuming that typical discharge voltages for argon, krypton and xenon would be less than 50, 35, and 35 V, respectively. If it is further assumed that the centerline to average value of I^{++}/I^{+} is about 1.5, the values of m_β and n_{0D}, based on the centerline value of β, would change by less than 2 percent from values obtained using the average value of β.

A value of β greater than 0.95 results if component lifetime considerations dictate that the double to single charged ion ratio be less than 10 percent. These constraints impose discharge voltages less than about 50, 35, and 35 V for argon, krypton, and xenon, respectively. The uncertainties in m_β and n_{0D} without any correction for charge state effects will certainly be less than 5 percent. The thrust correction due to doubly charged ions can be expressed as:

$$\alpha = 0.586\beta + 0.414 \tag{4}$$

where neglecting triply ionized species is a reasonable assumption for most practical operating conditions. With the discharge voltage constraints imposed, the thrust correction factor for doubly charged ions will be greater than 0.96. For thruster optimization studies where the stated discharge voltage guidelines are followed, extensive charge-state documentation of ring-cusp thrusters may not be required because the thrust value determined from electrical parameters is reduced by less than 4 percent, due to charge-state effects.

Thruster Performance with Ion Extraction

Thruster performance evaluation with ion beam extraction was conducted with line-cusp and ring-cusp devices using argon, xenon, and krypton propellants. All the data presented are corrected for vacuum facility gas ingestion into the thruster discharge chamber. Ion beam current corrections for multiply ionized species were made by assuming the ratio of doubly (or triply) ionized species was equal to the centerline values.

Figure 5 compares the performance of past and present argon thruster configurations. Maximum argon beam currents for these curves are in the range 2.5 to 7 A. It can be seen that the J-series 30-cm-diameter divergent field thruster outperforms the two line-cusp thrusters at about a 0.77 propellant efficiency (ref. 1). The maximum argon propellant efficiency for the divergent field thruster is unknown.

The minimum ion beam production cost was about 200 W/A and 140 W/A for the 17-cm-diameter line-cusp thruster and the 26-cm-diameter LC1, respectively. The reduction in ion production costs may simply be associated with effects produced by variations in discharge chamber length to diameter ratio. For example, reference 9 estimates the ion-beam production costs to be approximately proportional to [1 + (21/d)] for cylindrical discharge chambers. The smaller diameter thruster had an l/d of about 1.4 and the 26-cm-diameter thruster's l/d was about 0.6. Using the relationship of reference 9, a minimum ion-beam production cost of about 120 W/A might have been expected by using the larger line-cusp thruster.

The ion-beam production cost, at 0.9 propellant efficiency, was reduced by about a factor of two by changing from the line-cusp to a ring-cusp configuration. Tests without ion extraction qualitatively predicted this result. The difference in performance was primarily attributed to higher ion wall losses measured in the upstream end of the line-cusp discharge chamber.

Thruster RC3 showed a reduction in ion-beam production costs over RC1 of about 25 W/A to a value of 112 W/A at a propellant efficiency of 0.9. Other detailed parameters for thruster RC3 at an argon propellant efficiency of 0.9 are: discharge voltage, 48 V; anode current, 23 A; ion beam current, 6.5 A; cathode/main flow role, 0.7 A/6.5 A; and a centerline ratio of doubly to single charged ions of 8 percent.

Based on the results of tests without ion extraction, it was apparent that thruster RC3, Mod. 2 was the most promising configuration. Subsequent tests of this discharge chamber with beam extraction resulted in a number of unstable situations, while throttling and a minimum discharge voltage of 40 V for any cathode flow rate. Final evaluation, with beam extraction, involved retreating to thruster RC3 which was stable over a wide range of flow rates and had a minimum discharge voltage of 34 V with argon propellant.

Figure 6 shows the performance of thruster RC3 for three argon flow rates as well as with xenon and krypton. The base level ion-beam production cost is nearly independent of propellant type and was about 100 W/A. Highest performance was obtained with xenon where the ion-beam production cost was 95 W/A at 0.95 propellant efficiency. Some small uncertainties in the xenon and krypton flow rates do exist, however, since the flow rate transducers were directly calibrated only with argon.

The maximum beam currents, reported in Fig. 6, were obtained at a total accelerating voltage of about 1800 V. The maximum ion-beam currents at this total accelerating voltage were 6.6, 5.4, and 4.4 A for argon, krypton and xenon, respectively.

Table V shows thruster-performance values for the ring-cusp thruster using twoand three-grid ion optics. Basic equations used in the performance calculations are shown in appendix A. Table V(a) consists primarily of measured parameters with estimated values of neutralizer functions, fixed power losses, and thrust-reduction factor due to beam divergence. The specific impulse range for the two-grid ion optics was from about 3000 to 7000 sec. Table V(b) shows the projected performance parameters based on

the discharge chamber data of table V(a) and the use of a three-grid ion optics system, which is presently under development (ref. 10). In this case, operation at a beam voltage of 400 V would yield specific impulse values from about 1600 to 4000 sec. The data in table V for the 30-cm-diameter thruster, using either argon, krypton or xenon, cover a range of 1.6 to 10 kw input thruster power and thrust levels from 100 to 250 mN.

Figure 7 shows that about a 50 percent gain in thrust to power ratio can be obtained by the use of three-grid ion optics. Thrust to power ratios from 20 to 60 mN/kw can be obtained at values of specific impulse from 7000 to 2000 sec by the appropriate choice of propellant type, input power, and type of ion optics. Typical values of overall thruster efficiency, using the two-grid ion optics at high specific impulse, was 0.70 to 0.80, while operation at low specific impulse, using three-grid ion optics, would potentially produce an overall thruster efficiency of about 0.60.

CONCLUSIONS

A 30-cm-diameter ring-cusp ion thruster was investigated to reduce ion-wall losses and provide a high ion flux towards the ion optical system. The thruster delivered inert gas ion beam currents up to about 7 A, with significant improvements in discharge chamber performance over conventional divergent field thrusters. The thruster has strong boundary ring-cusp magnetic fields, a diverging field in the cathode region, and a nearly field-free volume upstream of the ion extraction system. Magnet rings were attached to a iron shell at anode potential.

Without ion beam extraction, the ring-cusp device reduced ion-wall losses between cusps by at least a factor of two, over a line-cusp thruster of the same diameter. The ring-cusp chamber was optimized such that ion-current densities at the walls in the upstream half of the discharge chamber and at chamber walls between cusps were less than 7 percent of the ion-current densities at the ion-extraction plane. Nearly 100 percent of the electron current was collected by the two downstream magnet rings and the downstream pole piece which was at anode potential. Results of ion-extraction tests with the ring-cusp thruster were consistent with the chamber wall probe data obtained without ion-extraction and showed nearly a factor of two improvement in ion-beam production costs over the line-cusp device. Minimum ion-beam production costs were found to be nearly independent of propellant type and were in the range 90 to 100 W/A. Propellant efficiences in excess of 0.90 were achieved at 95 to 120 W/A for the three inert gases.

With a given propellant, the thrust-to-power ratio of thrusters using two-grid ion optics can potentially be increased by about 50 percent by the use of three-grid ion optics. The full range of thrust-to-power ratios, from 20 to 60 mN/kw, can be obtained at values of specific impulse, from 2000 to 7000 sec, by the appropriate choice of propellant type, input power, and type of ion optics.

Beam-ion charge state measurements taken with an ExB spectrometer probe indicate that if the ratio of doubly to singly charged ions is to be less than about 10 percent, due to component lifetime considerations, discharge voltages for argon, krypton, and xenon should generally be less than 50, 35,

and 35 V, respectively. Under these conditions, the charge state corrections to the measured ion mass flow rate and thrust should be less than 5 percent and 4 percent, respectively. Further, given comparable discharge parameters, the inert gas ring-cusp thruster will exhibit less centerline screen-grid erosion than the divergent field thruster because of a relatively lower concentration of doubly-charged ions on centerline.

APPENDIX A

The following equations were used in the calculation of the performance parameters in table V:

. Ideal thrust

$$T_I = \sqrt{2\left(\frac{m}{e}\right)}\ J_B \sqrt{V_B} \tag{A1}$$

where $$V_B = V_s + V_D - V_N \tag{A2}$$

. Actual thrust

$$T_A = \gamma\ T_I \tag{A3}$$

where $$\gamma \simeq \alpha\ F_T \tag{A4}$$

. Propellant mass flow rate

$$\dot{M}_o = \left(\frac{M}{e}\right) \dot{m}_o \tag{A5}$$

where $$\dot{m}_o = \dot{m}_M + \dot{m}_c + \dot{m}_N + \dot{m}_I \tag{A6}$$

. Specific impulse

$$I_{sp} = \frac{T_A}{\dot{M}_o g} \tag{A7}$$

. Input power

$$P \simeq V_s\ J_B + V_D\ J_D + P_F \tag{A8}$$

where P_F includes power associated with the accelerator, heater,

and neutr: izer supplies.

. Overall thruster efficiency

$$\eta_T = \frac{1}{2} \frac{TA^2}{\dot{M}_o P} \tag{A9}$$

or

$$\eta_T = \frac{\eta_u' \gamma^2}{1 + 2\left(\frac{e}{M}\right)\left(\frac{\eta_u' \gamma}{g I_{sp}}\right)^2\left(\epsilon' + V_N + \frac{P_F}{J_B}\right)} \tag{A10}$$

where $$\epsilon' = \frac{V_D (J_D - J_B)}{J_B}, \ W/A \tag{A11}$$

and $$\eta_u' = \frac{J_B}{\dot{m}_o} \tag{A12}$$

The parameter η_T is defined to be the overall thruster efficiency and does not include losses associated with power processing or power transmission.

REFERENCES

1. Rawlin, V.K., "Operation of the J-Series Thruster Using Inert Gases," AIAA Paper 82-1929, Nov. 1982.
2. Sovey, J.S., "Performance of a Magnetic Multipole Line-Cusp Argon Ion Thruster," Journal of Spacecraft and Rockets, Vol. 19, No. 3, May-June 1982, pp. 257-262.
3. Ramsey, W.D., "Magnetelectrostatic Thruster Physical Geometry Tests," AIAA Paper 81-0753, Apr. 1981.
4. Moore, R.D., "Magneto-Electrostatically Contained Plasma Ion Thruster," AIAA Paper 69-260, Mar. 1969.
5. Forrester, A.T., Goebel, D.M., and Crow, J.T., "IBIS-A Hollow-Cathode Multipole Boundary Ion Source," Applied Physics Letters, Vol. 33, July 1978, pp. 11-13.
6. Rawlin, V.K., "Sensitivity of 30-cm Mercury Bombardment Ion Thruster Characteristics to Accelerator Grid Design," AIAA Paper 78-668, Apr. 1978.
7. Vahrenkamp, R.P., "Measurement of Double Charged Ions in the Beam of a 30-cm Mercury Bombardment Thruster," AIAA Paper 73-1057, Oct. 1973.
8. Vahrenkamp, R.P., "An Experimental Investigation of Multiple Ion Processses in Mercury Bombardment Thrusters," AIAA Paper 75-397, Mar. 1975.
9. Beattie, J.R., and Wilbur, P.J., "Cusped Magnetic Field Mercury Ion Thruster," Journal of Spacecraft and Rockets, Vol. 14, No. 12, Dec. 1977, pp. 747-755.
10. Rawlin, V.K., and Hawkins, C.E., "Increased Capabilities of the 30-cm Diameter Hg Ion Thruster," NASA TM-79142, May 1979.

TABLE I. - CUSP-FIELD THRUSTER PARAMETERS

Thruster (a)	Ion extraction diameter, cm	Cylindrical shell length, cm	Cylindrical shell diameter, cm	Number of magnet rows or rings on cylindrical wall	Magnet ring axial location from downstream anode shell, cm	Magnet field strength, T	Magnet ring radial location from thruster centerline on backplate, cm	Magnet field strength, T	Cathode magnet strength and polarity at cathode tip, T	Cathode tip position from downstream end of anode shell cm	Downstream pole piece inner diameter,[d] cm
LC1	25.7	27.9	27.9	(b)12	--	--	--	--	0.021 S	14.0	--
RC1	25.7	27.9	27.9	4	6.2 9.3 14.6 22.9	0.24 .24 .24 .24	6.2 10.8	0.24 .24	0.018 N	18.7	25.7
LC2	28.3	26.7	34.3	(b)24	--	--	--	--	0.022 N	19.7	--
LC3	28.3	26.7	34.3	(b)16	--	--	--	--	0.022 N	19.7	--
RC2	28.3	26.7	34.3	3	3.8 11.4 22.9	0.24 .24 .24	6.8 15.2	0.24 .24	0.020 N	17.8	28.3
RC2 Mod 1	28.3	26.7	34.3	3	3.8 11.4 22.9	0.24 .32 .32	6.8 15.2	0.32 .32	0.030 N	17.8	28.3
RC3 (c)	28.3	26.7	34.3	3	3.8 11.4 22.9	0.24 .24 .24	6.8 15.2	0.24 .24	0.020 N	17.8	28.3
RC3 Mod 1 (c)	28.3	26.7	34.3	3	3.8 11.4 22.9	0.24 .32 .32	6.8 15.2	0.32 .32	0.030 N	17.8	28.3
RC3 Mod 2 (c)	28.3	26.7	34.3	3	3.8 11.4 22.9	0.24 .24 .32	6.8 15.2	0.32 .32	0.030 N	17.8	28.3

a LC denotes Line cusp; RC denotes Ring cusp.
b Backplate magnet configuration for 12 rows of magnets, Typical

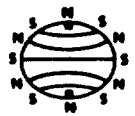

c A magnet ring (field strength, 0.24 T) whose outside diameter was 33-cm, was positioned on the downstream pole piece.
d Downstream pole piece, at anode potential.
e Magnets are 35 percent samarium - 65 percent cobalt, 1.3 x 1.9 x 0.5 cm.

TABLE II. - COMPARISON OF GRID-PLANE ION CURRENTS OBTAINED FROM BIASED PROBES

Thruster configuration	Ion current at grid plane, A	Change in grid plane ion current over thruster, RC2, percent	Flatness parameter, ratio of average to centerline current density
LC2	11.5	-21	0.71
LC3	11.8	-19	.64
RC2	14.6	---	.61
RC2 Mod 1	16.2	+11	.69
RC3	14.6	0	.76
RC3 Mod 1	16.9	+16	.67
RC3 Mod 2	16.9	+16	.80

Discharge parameters, V_D = 40V, $|J_C| + |J_G|$ = 42A; typical flow rates $\dot{m}_C$ = 1.3A, $\dot{m}_m$ = 6 A, $\dot{m}_I$ = 6 A (estimated), no high voltage ion extraction. Grid at cathode potential.

TABLE III. - CURRENTS TO PROBES LOCATED IN THE RING-CUSP THRUSTER CHAMBER (RC3, Mod 2)

Probe number	Probe location	Ion current,[a] mA	[b]Electron current, A
1	Grid	43	----
2	Grid	41	----
3	Grid	30	----
4	Between cusps[c]	3	0.03
5	Cusp[d] Cusp[e]	13 5	0.8 0.3
6	Between cusps[c]	2	0
7	Cusp[d] Cusp[e]	14 5	1.0 0.3
8	Between cusps[c]	1.5	0
9	Cusp[d]	0.6	0
10	Cusp[d]	0.3	0
11	Cusp[d]	0.8	0
	Downstream pole piece	1600	10

Probe diameter: 1.3 cm.
Discharge parameters: $\dot{m}_C$ = 1.3 A, $\dot{m}_M$ = 6 A, $\dot{m}_I$ = 6 A, V_D = 40 V, $|J_C| + |J_G|$ = 42 A.
[a] Probe bias = -30 V, grid at cathode potential.
[b] Probe at anode potential.
[c] Probe located 1.8 cm above anode shell.
[d] Probe located 1.2 cm above magnet.
[e] Probe located 0.05 cm above magnet.

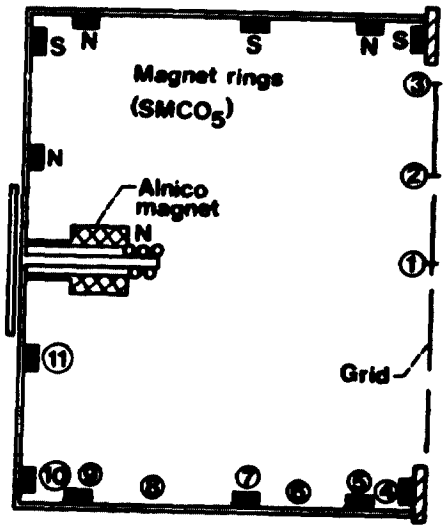

TABLE IV. - CHARGE-STATE VARIATIONS WITH RADIUS FOR THRUSTER RC3.

Propellant	Discharge voltage, V	Discharge current, A	Measured beam current, A	Ratio of doubly to singly charged ion current, I^{++}/I^{+}			R(average)	$\frac{R(C/L)}{R(average)}$
				Centerline	0.5 Rad.	0.8 Rad.		
Argon	46.7	12.4	4.9	0.060	0.060	0.040	0.047	1.3
Xenon	41.5	12.3	4.9	.34	.25	.18	.22	1.6

TABLE V. - PROJECTED RING-CUSP THRUSTER PERFORMANCE WITH INERT GAS PROPELLANTS USING TWO TYPES OF ION OPTICS

[Assumptions: V_N = 20 V; P_F = 40 W; m_N = 0.10 A; F_I = 0.98 (table (a)); F_T = 0.95 (table (b)).]

(a) Performance with two-grid ion optics

Gas	Beam voltage, V_B, V	Beam current, J_B, A	Discharge voltage, V_D, V	Ion beam production ϵ', W/A	Overall propellant nu	Ion mass flowrate correction factor, β	Thrust correction factor, α	Thruster input power, P, W	Thrust, T_A, N	Specific impulse, I_{sp}, sec	TA/P, mN/kW	Overall thruster efficiency, η_T
Ar	1340	5.82	40.8	99.4	0.789	0.990	0.994	8 420	0.188	6270	22.3	0.686
	1440	6.61	46.1	109	.896	.975	.985	10 400	.221	7370	21.2	.767
	1340	6.79	48.3	114	.921	.968	.981	10 050	.220	7340	21.9	.787
Kr	1260	4.24	34.2	105	.861	.974	.985	5 900	.191	4560	32.4	.723
	1320	4.89	39.2	120	1.010	.925	.956	7 180	.219	5300	30.5	.791
	1320	5.40	46.1	143	1.110	.875	.927	8 030	.235	5680	29.3	.815
Xe	1150	3.04	29.4	90.5	.682	.985	.992	3 870	.165	2780	42.7	.581
	1200	3.95	32.8	91.8	.889	.965	.979	5 220	.217	3670	41.6	.746
	1240	4.43	35.6	94.6	.996	.940	.965	6 040	.244	4120	40.4	.814

(b) Projected performance with three-grid ion optics

Ar	400	5.82	40.8	99.4	0.789	0.990	0.994	3 060	0.100	3330	32.6	0.532
	400	6.51	46.1	109	.896	.975	.985	3 540	.112	3750	31.8	.585
	400	6.79	48.3	114	.921	.968	.992	3 670	.116	3880	31.7	.603
Kr	400	4.24	34.2	105	.861	.974	.985	2 270	.105	2500	46.2	.566
	400	4.89	39.2	120	1.010	.925	9.956	2 680	.117	2840	43.7	.608
	400	5.40	46.1	143	1.110	.875	.927	3 080	.126	3050	40.9	.611
Xe	400	3.04	29.4	90.5	.682	.985	.991	1 590	.094	1580	59.0	.459
	400	3.95	32.8	91.8	.889	.965	.979	2 060	.121	2050	58.7	.589
	400	4.43	35.6	94.6	.996	.940	.965	2 320	.135	2270	58.1	.647

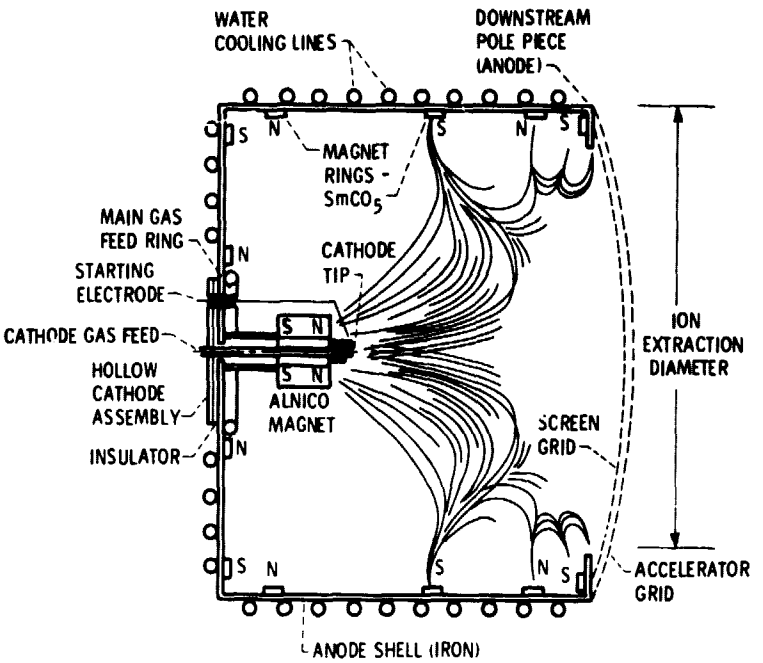

Figure 1. - Ring-cusp discharge chamber (RC3) with a sketch of an iron filing map.

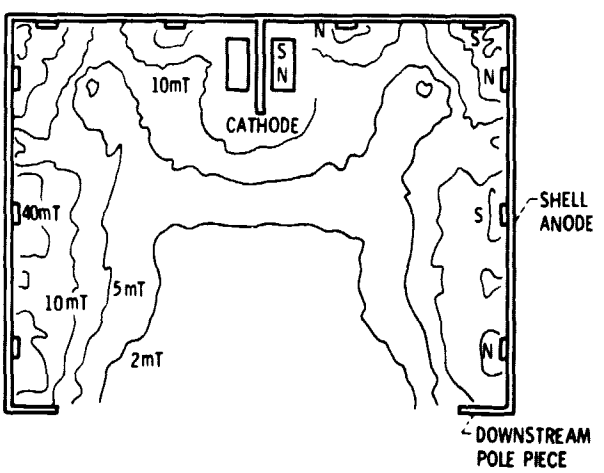

Figure 2. - Typical discharge chamber magnetic field contours-thruster RC2.

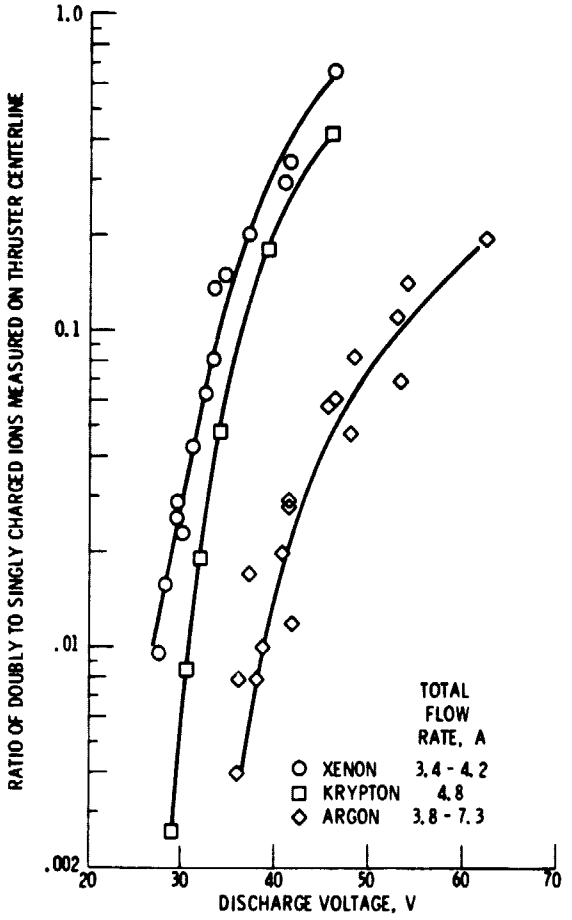

Figure 3. - Ratio of doubly to singly charged ions on thruster centerline versus discharge voltage.

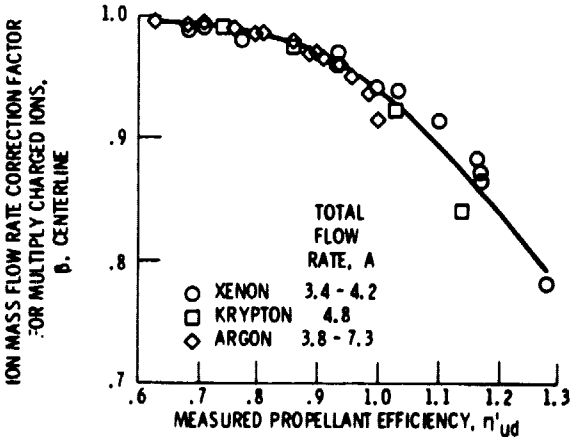

Figure 4. - Ion mass flow rate correction factor versus measured propellant efficiency for thruster RC3.

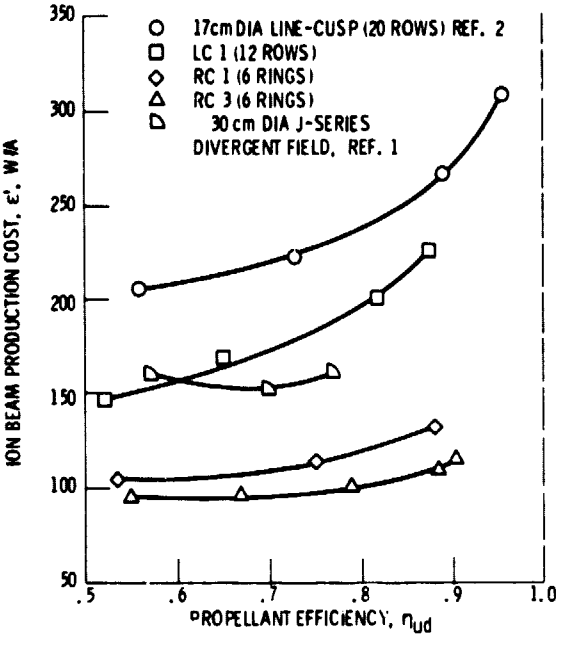

Figure 5. - Perfor...nce comparison of various argon thruster configurations.

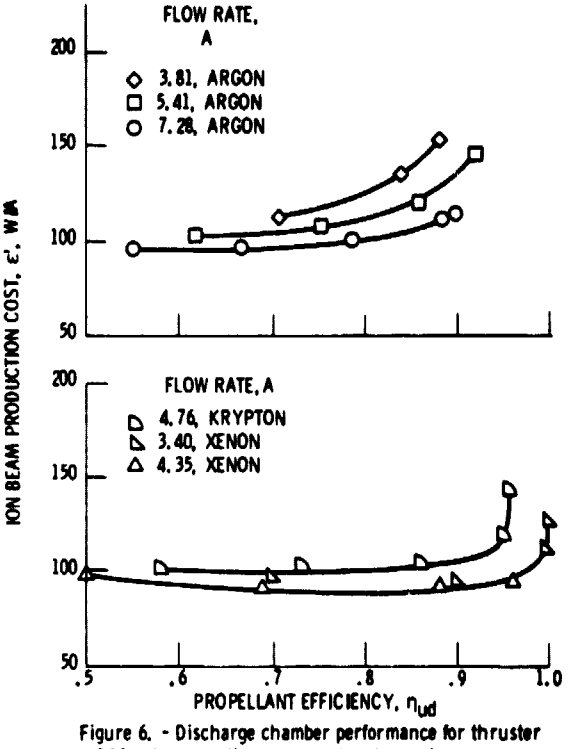

Figure 6. - Discharge chamber performance for thruster RC3 using propellants argon, krypton and xenon.

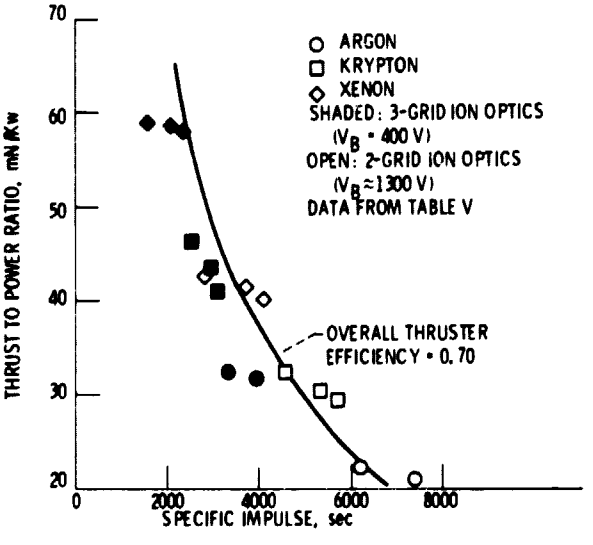

Figure 7. - Projected ring-cusp thruster performance with inert gas propellants using two types of ion optics.